ERRATUM

This article is reprinted in its entirety, with corrections, from *J Nucl Med* 21:971-977, 1980. The original manuscript and proofread galleys submitted by the author were correct. Errors introduced at a later stage resulted from the implementation of new software, for which the printer accepts full responsibility and deeply regrets any inconvenience caused to the author and the readers. This unusual problem has been fully corrected and will not occur again. Please place this insert in the October 1980 issue.

Method for Optimizing Side Shielding in Positron-Emission Tomographs and for Comparing Detector Materials

Stephen E. Derenzo

University of California, Berkeley, California

This report presents analytical formulas for the image-forming and background event rates seen by circular positron-emission tomographs with parallel side shielding. These formulas include deadtime losses, detector efficiency, coincidence resolving time, amount of activity, patient port diameter, shielding gap, and shielding depth. A figure of merit, defined in terms of these quantities, describes the signal-to-noise ratio in the reconstructed image of a 20-cm cylinder of water with uniformly dispersed activity. For 1-cm-wide NaI(Tl) detectors, a 50-cm patient port, an activity of 200 μCi per axial centimeter, and a shielding gap of 2 cm, the optimum shielding depth is 20 cm, which requires a detector circle diameter of 90 cm. For a 25-cm patient port and other conditions as above, the optimum shielding depth is 14 cm. Results are presented for the scintillators NaI(Tl), bismuth germanate (BGO), CsF, and plastic; and for Ge(Li) and wire chambers with converters. In these examples, BGO provided the best signal-to-noise for activity levels below 1000 μCi per cm, and CsF had the advantage for higher activity levels.

J Nucl Med 21: 971-977, 1980

In positron-emission, transverse-section tomography, the image is derived from the detection of unscattered coincident annihilation pairs. Almost all positron-emission tomographs use shielding on either side of the detector plane to block activity external to the transverse section being imaged (*1-8*). Shielding is also used between detector planes in multiple-section devices (*9-15*). In spite of this shielding, image contrast is degraded by true coincidences of scattered annihilation pairs and by accidental coincidences of unrelated annihilation photons (Fig. 1). Most positron-imaging systems operate with scattered and accidental backgrounds that are each typically 20% of the detected coincidences. Even if these backgrounds can be perfectly estimated and subtracted from the detected coincidences, the random fluctuations in the result are greater than if the backgrounds did not exist. In the following sections we examine the trade-off between sensitivity and backgrounds and describe a procedure for determining the optimum shielding depth for single-ring circular positron-emission tomographs. This treatment does not consider, but can be extended to include, nonparallel shields and multislice configurations.

The procedure consists of (a) measuring image and background event rates from a 20-cm phantom using the type of detector system being considered; (b) fitting analytical expressions to these rates; and (c) varying the shielding depth in those expressions to maximize the statistical accuracy in the reconstructed image.

As an example, this procedure is carried out for circular detector arrays using the Donner 280-Crystal positron tomograph with NaI(Tl) and bismuth germanate (BGO) detectors. Since the results depend significantly on detector characteristics, additional examples are provided for a variety of detectors, using typical

Received Nov. 5, 1979; revision accepted June 18, 1980.

For reprints contact: Stephen E. Derenzo, PhD, Donner Laboratory, University of California, Berkeley, CA 94720.

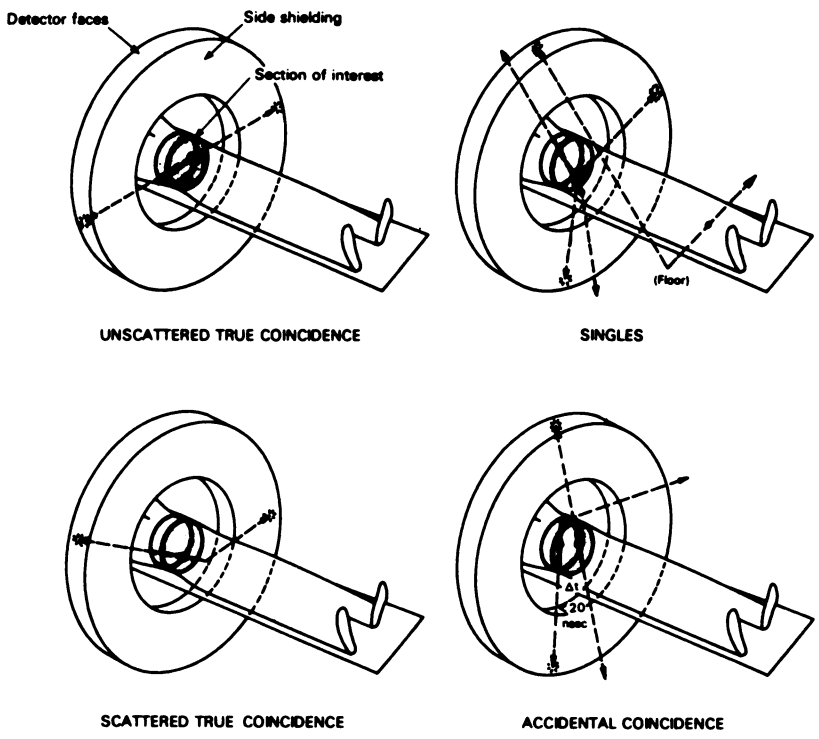

FIG. 1. Types of coincident events detected by positron tomographs. Image is formed from unscattered coincident annihilation pairs. Coincident scattered pairs and accidental coincidences of unrelated photons result in broad backgrounds.

values of detection efficiency and of time and energy resolution.

EVENT RATES

As has been shown analytically for circular positron-emission tomographs (*16*), the overall rate of unscattered coincident events (C_I) is given by:

$$C_I = B_I \epsilon^2 \rho G_e^2/(H + \tfrac{1}{2}P) \qquad (1)$$

where ϵ is the detection efficiency for annihilation photons (including detector packing fraction), ρ is the activity density in μCi per axial centimeter, G_e is the effective shielding gap (cm), H is the shielding depth (cm), P (Fig. 2) is the patient port diameter (cm), and B_I is a constant that incorporates the average attenuation and numerical factors. $R = H + \frac{1}{2}P$ is the detector ring radius. For activity distributed in a 20-cm cylinder of water, B_I = (37,000 $sec^{-1}\mu Ci^{-1}$) × (average attenuation) × (1/4) = 1850 $sec^{-1}\mu Ci^{-1}$. Due to edge penetration, the effective shielding gap, G_e, is slightly larger than the physical shielding gap, G:

$$G_e = G + \delta_G. \qquad (2)$$

A different analytical expression was derived in (*16*) for the overall rate of coincident scattered events (C_S):

$$C_S = \frac{B_S \epsilon^2 \rho G_e^3}{H(H + \frac{1}{2}P)} \qquad (3)$$

where H is the shielding depth in centimeters and B_S is a constant that incorporates pulse-height thresholds, the angular distribution of accepted Compton scatters, and numerical factors.

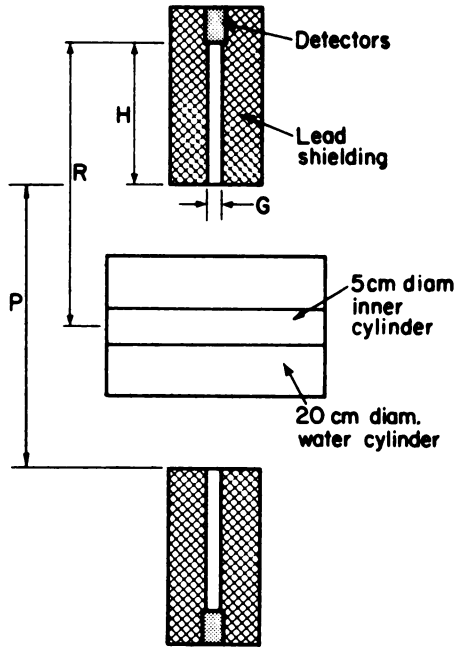

FIG. 2. Detector, shielding, and phantom geometry for optimization calculations. Scatter background can be measured in inner cylinder by imaging with activity in outer cylindrical annulus only.

The overall rate of accidental events (C_A) given in (*16*) is:

$$C_A = B_A \epsilon^2 \tau \rho^2 G_e^4 / H^2, \quad (4)$$

where τ is the full coincidence-time window in nanoseconds, and B_A is a constant that incorporates pulse-height thresholds, detector efficiencies for scattered and unscattered photons, and numerical factors.

These rates are reduced by system deadtime, which is a combination of the deadtime of the detectors, the timing and pulse-height discriminators, the coincidence circuits, and memory. We assume that for a particular scattering medium (i.e., a 20-cm cylinder of water) the ratio of photon interactions to coincident events is fixed, and that we can define an effective nonparalyzing system deadtime that applies to the total coincident-event rate only. Before deadtime losses, the system detects C_I C_S C_A in the on-time coincidence window and C_A in an off-time window. Thus the total coincidence rate is $C_T = C_I\ C_S\ 2C_A$, and the fraction of events, F, that is lost to deadtime is given by:

$$F = tC_T/(1\ tC_T), \quad (5)$$

where t is the deadtime per event. The observed system rates are:

$$D_I = (1 - F)C_I$$
$$D_S = (1 - F)C_S$$
$$D_A = (1 - F)C_A. \quad (6)$$

In the central region of the reconstructed image of a cylinder of activity in water, the intensity of unscattered coincident events per square centimeter (d_I) is given by:

$$d_I = (1 - F)b_I \epsilon^2 \rho G_e^2/(H + \tfrac{1}{2}P). \quad (7)$$

For a 20-cm cylinder, $b_I = 29.44$ reconstructed events $sec^{-1}\ cm^{-2}\mu Ci^{-1}$. The intensity of scattered coincident events per square centimeter (d_S) is given by:

$$d_S = \frac{(1 - F)b_S \epsilon^2 \rho G_e^3}{H(H + \frac{1}{2}P)}, \quad (8)$$

and the intensity of accidental events per square centimeter (d_A) is given by:

$$d_A = (1 - F)b_A \epsilon^2 \tau \rho^2 G_e^4 / H^2. \quad (9)$$

Before background subtraction, the total intensity, d_T, is given by:

$$d_T = d_I\ d_S\ d_A. \quad (10)$$

DEFINITION OF THE FIGURE OF MERIT

A figure of merit (Q) can be defined as the product of the unscattered coincidence rate (D_I) and the image contrast (d_I/d_T) using the arguments of Beck (*17*):

$$Q = D_I(d_I/d_T) \quad (11)$$

Q may also be called an "effective" image event rate, since the same signal-to-noise ratio would be obtained in an ideal tomograph with $D_I' = Q$ and $d_S' = d_A' = 0$. Note that d_I, d_S, and d_A all undergo the same deadtime effects, attenuation correction, and error propagation in the reconstruction process.

From Ref. *18*, it is possible to relate the value of Q (and the imaging time, T) to the statistical uncertainty in the reconstructed image. In the case of a 1-cm^2 cell near the center of a 20-cm cylinder of uniform activity, the fractional rms uncertainty is given by $90/\sqrt{QT}$.

OPTIMIZATION OF THE FIGURE OF MERIT

Equations 1-10 show that for a given imaging situa-

TABLE 1. SHIELDING OPTIMIZATION FOR NaI(Tl)*

H Shielding depth (cm)	D_T Observed total† (sec^{-1})	F Deadtime loss (%)	D_I Image event rate (sec^{-1})	d_S/d_I Scatter/image ratio	d_A/d_I d_I/d_T Accid./image ratio	Q Image contrast	Quality factor (sec ins1)
5	118,582	11.9	8,805	0.97	2.59	.22	1,932
10	40,000	4.0	8,220	0.48	0.76	0.45	3,672
15	22,350	2.2	7,325	0.32	0.38	0.59	4,295
20‡	15,352	1.5	6,558	0.24	0.24	0.67	4,418
25	11,718	1.2	5,924	0.19	0.17	0.73	4,337
30	9,513	1.0	5,397	0.16	0.13	0.77	4,175
40	6,971	0.7	4,579	0.12	0.09	0.83	3,789
50	5,541	0.6	3,974	0.10	0.06	0.86	3,422
60	4,617	0.5	3,510	0.08	0.05	0.88	3,102

* Port = 50 cm, effective shielding gap, G_e = 2 cm, pulse-height threshold = 100 keV, detector efficiency ϵ = 45%, ρ = 200 μCi/cm, deadtime t = 1 μsec, coincidence-time window τ = 15 nsec.

† Total rate in on-time and off-time coincidence windows combined.

‡ H = 19.8 cm for maximum Q.

tion, reducing the shielding depth, H, improves the imaging rate, D_I, but also decreases the image contrast, d_I/d_T. Choosing a value of H that maximizes Q (Eq. 11) ensures the best tradeoff between sensitivity and image contrast.

By combining Eqs. 1-11 we show the dependence of Q on the shielding depth, H:

$$Q(H) = \frac{A_6H^4}{A_0 + A_1H + A_2H^2 + A_3H^3 + A_4H^4 + A_5H^5}, \quad (12)$$

where

$$A_6 = B_Ib_I\epsilon^2\rho G_e^2$$

$$A_5 = b_I$$

$$A_4 = b_sG_e\, b_IP/2\ \rho G_e^2(tB_Ib_I\epsilon^2\, b_A\tau)$$

$$A_3 = G_e[b_a\tau\rho G_eP/2 + (tb_I\epsilon^2\rho G_e^2) \times (B_S + B_A\tau\rho G_e) + (P/2 + tB_I\epsilon^2\rho G_e^2) \times (b_S + b_A\tau\rho G_e)]$$

$$A_2 = \rho G_e^2(b_A\tau P/2)\ (P/2 + B_It\epsilon^2\rho G_e^2)\ t\rho\epsilon^2G_e^4[B_Ab_I\tau\rho P/2 + (B_S + B_A\tau\rho G_e)(b_S + b_A\tau\rho G_e)]$$

$$A_1 = (t\tau\epsilon^2\rho^2G_e^5P/2)\ [b_A(B_S + B_A\tau\rho G_e) + B_A(b_S + b_A\tau\rho G_e)]$$

and

$$A_0 = B_Ab_At\tau^2\epsilon^2\rho^3G_e^6P^2/4. \quad (13)$$

The slope of Q is given by:

$$\frac{dQ}{dH} = \frac{A_6H^3[4A_0 + 3A_1H + 2A_2H^2 + A_3H^3 - A_5H^5]}{[A_0 + A_1H + A_2H^2 + A_3H^3 + A_4H^4 + A_5H^5]^2}. \quad (14)$$

An analytical expression for an optimum value of H (i.e., a formula for H in terms of A_0, A_1, A_2, A_3, and A_5 such that $dQ/dH = 0$) requires the general solution to the quintic equation, which has not been accomplished. However, since the coefficients $A_0, \ldots, A_6$ are positive, it may be shown from Eq. 14 that the slope of Q is equal to zero for only one value of H, is greater than zero for smaller values of H, and is less than zero for larger values of H. As a result Q has only one extremum—a maximum.

In this work the optimum value of H was determined in each case by using an iterative quadratic interpolation algorithm on a small digital computer.

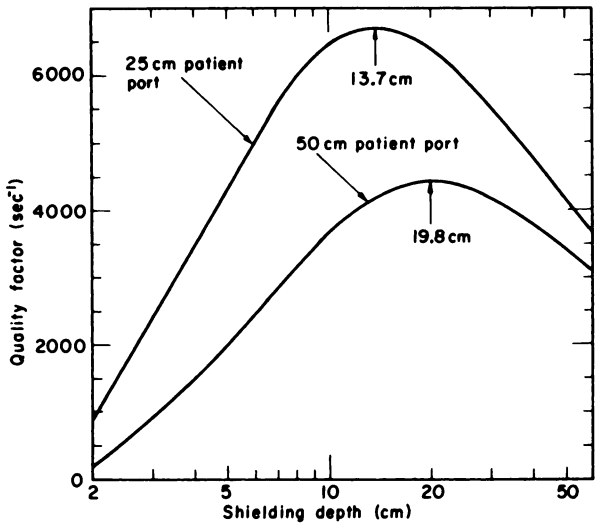

FIG. 3. Effective event rate, Q, as function of shielding depth for NaI(Tl) detectors with 45% detection efficiency, 2-cm shielding gap, 200 μCi/cm, 1-μsec deadtime, and coincidence resolving time of 15 nsec. Optimum values are indicated with arrows for 25- and 50-cm patient ports.

EXAMPLES

NaI(Tl). The constants ϵ, B_S, B_A, b_S, b_A, and the penetration factor δ_G were determined for NaI(Tl) by fitting Equations 1-9 to measurements of 20-cm phantoms made by the Donner 280-crystal positron tomograph. The overall rates D_I, D_S, and D_A were measured for a 20-cm-diameter cylinder of activity in water (δ), and $d_S/(d_S + d_I)$ and $d_A/(d_S + d_I)$ were measured at the center of reconstructed images of a 5-cm-diameter cylinder containing only water, surrounded by a 20-cm-diameter annulus of activity in water (Fig. 2). The pulse-height threshold was 100 keV, the coincidence-time window was 20 nsec, the activity was varied from 100 to 300 μCi/cm, and the shielding gap was varied from 1 to 3 cm. A good fit was obtained with $\epsilon = 45\%$, $B_S = 5100$, $B_A = 0.73$, $b_S = 71$, $b_A = 5.3 \times 10^{-3}$, and $\delta_G = 2.1$ mm. The penetration factor δ_G was necessary in each of Equations 1, 3, and 4 (D_I, D_S, and D_A, respectively) for an adequate fit to the data. Using these coefficients in Eqs. 1-10, the shielding depth, H, was varied to maximize the figure of merit, Q, in Eq. 11.

As an example, Table 1 lists D_I, d_S/d_I, d_A/d_I, d_I/d_T, and Q as a function of shielding depth, H, for a 50-cm patient port, $\rho = 200$ μCi/cm, $G_e = 2$ cm effective shielding gap, a 20-cm-diameter water cylinder, and a 1-μsec deadtime. Figure 3 presents curves of Q as a function of H for the same conditions except for 25-cm and 50-cm patient ports.

Other detector materials. The relative rates D_I, D_S, and D_A for bismuth germanate (BGO) detector crystals have been measured in this system with a 300-keV pulse-height threshold (δ), and led to the constants $\epsilon = 67\%$, $B_S = 5100$, $B_A = 0.36$, $b_S = 71$, $b_A = 2.6 \times 10^{-3}$. Note that the photopeak selection reduces B_A and b_A, but not B_S and b_S, since the scatter background consists

TABLE 2. OPTIMUM VALUES OF H AND Q FOR VARIOUS DETECTOR MATERIALS*

	NaI(Tl)	BGO	CsF	Ge(Li)	Wire-chamber converters	Plastic
Pulse-height threshold:	100 keV	300 keV	100 keV	500 keV	200 keV	100 keV
511-keV efficiency:	45%†	67%†	50%† 15%†	20%	20%†	
Coincidence-time window:	15 ns	30 ns	3.3 ns	15 ns	50 ns	3.3 ns
B_S	5,100	5,100	5,100	0	5,100	5,100
B_A	0.73	0.36	0.73	0.15	0.50	0.73
b_S	71	71	71	0	71	71
b_A	5.3×10^{-3}	2.6×10^{-3}	5.3×10^{-3}	1.0×10^{-3}	3.5×10^{-3}	5.3×10^{-3}
ρ = 100 μCi/cm						
Shielding depth: H (cm)	16.3	16.5	12.7	6.9	19.8	12.5
Image contrast: d_I/d_T	0.68	0.69	0.70	0.88	0.66	0.69
Quality factor: Q (sec^{-1})	2,460	5,417	3,390	459	435	546
ρ = 200 μCi/cm						
Shielding depth: H (cm)	19.8	20.3	14.1	8.9	24.7	13.8
Image contrast: d_I/d_T	0.67	0.68	0.70	0.85	0.63	0.69
Quality factor: Q (sec^{-1})	4,419	9,648	6,477	835	750	1, 1
ρ = 500 μCi/cm						
Shielding depth: H (cm)	27.6	29.4	17.6	12.5	34.6	16.7
Image contrast: d_I/d_T	0.65	0.67	0.70	0.80	0.58	0.68
Quality factor: Q (sec^{-1})	8,846	18,858	14,450	1,775	1,42 2,399	
ρ = 1000 μCi/cm						
Shielding depth: H (cm)	37.9	42.1	22.4	16.4	46.4	20.4
Image contrast: d_I/d_T	0.63	0.66	0.70	0.76	0.53	0.67
Quality factor: Q (sec^{-1})	13,827	28,561	24,894	3,031	2, 9	4,284

* Port = 50 cm, effective shielding gap G_e = 2 cm, deadtime t = 1 μsec per coincident event.
† Detector size 1 cm wide × 5 cm deep.

primarily of photons above 415 keV that have scattered through <40° (*5*).

By using the values for efficiency, time resolution, and energy resolution for other detector materials, it is possible to optimize the shielding depth for each material. Table 2 lists the results for six detector materials at four activity levels. See (*19*) for a more extensive tabulation. The detection efficiency for Ge(Li) and plastic was determined from Monte Carlo calculations that traced the interactions of a beam of 511-keV photons through a group of 1-cm-wide detectors (*20*). The detection efficiency was defined as the fraction of incident photons that produced a signal above threshold in only one detector.

Note that Table 2 was intended to provide examples of results of the optimization method only for a variety of detector materials, and does not necessarily represent the best that can be done.

DISCUSSION

In the examples considered in Table 2 (a circular detector array, parallel shields with a 2-cm gap, and a 50-cm patient port) the highest optimum value of Q is achieved with BGO at each of the four activity levels. The second best material is CsF, which has a lower detection efficiency than BGO but significantly better time resolution.

Ge(Li) is unique in having sufficient energy resolution to reject almost all tissue-scattered photons. This eliminates the coincident scattered background and greatly reduces the accidental background. The low full-energy efficiency for 511-keV photons, however, results in low values of Q.

Plastic scintillators are unique in having such excellent timing resolution that the coincidence-time window of 2–3 nsec is determined by the size of the patient port and the speed of light. If time resolutions of the order of ±100 psec could be realized for tomographic systems, the timing information and the use of shorter detectors could localize the annihilation point along the line of flight to ±1.5 cm. This possibility was suggested by Anger in 1966 (*21*) and is used in a 3-dimensional imaging system built by Nickles and coworkers (*22*). The use of CsF for time-of-flight positron tomography has been suggested by Allemand et al. (*23*) and by Mullani et al (*24*). In Ref. *23* a 0.5-nsec FWHM timing resolution is reported, and this is estimated to improve the signal-to-noise ratio in the reconstructed image of a 32-cm cylinder of activity in water by a factor of 2.9.

For the case of wire chambers with lead converters, rather optimistic values of efficiency and time resolution have been used, but the resulting quality factors are still relatively low. The situation may improve, as several groups are investigating schemes to improve their properties (*25–28*).

CONCLUSIONS

For positron-emission tomographs, one can define a quality factor that describes the signal-to-noise ratio in the reconstructed image, and it is then possible to choose a side-shielding depth and detector-circle diameter that optimize the tradeoff between sensitivity and image contrast. The method requires knowledge of the scaling coefficients for the scattered and accidental background rates as well as an adequate description of the detectors being considered.

Under these conditions, the comparison of optimal quality factors permits a direct comparison of the suitability of different detector materials for positron-emission tomography in terms of the signal-to-noise ratio. This approach may be expanded to include nonparallel shields and multislice geometries.

ACKNOWLEDGMENTS

I thank T. F. Budinger, L. Carrol, and R. H. Huesman for helpful discussions and T. Vuletich for valuable technical assistance. This work was reported in part at the 26th Annual Meeting of the Society of Nuclear Medicine, Atlanta, Georgia, June 26–29, 1979.

This work was supported by the Div. of Biomedical Research of the U.S. Dept. of Energy under Contract No. W-7405-ENG-48 and by NIH Grant No. CA 17566-3.

REFERENCES

1. ROBERTSON JS, MARR RB, ROSENBLUM B, et al: Thirty-two crystal positron transverse section detector. In *Tomographic Imaging in Nuclear Medicine*, Freedman GS, Ed. New York, Society of Nuclear Medicine, 1973, pp 142–153
2. HOFFMAN EJ, PHELPS ME, MULLANI NA, et al: Design and performance characteristics of a whole-body positron transaxial tomograph. *J Nucl Med* 17:493–502, 1976
3. CHO ZH, COHEN MB, SINGH M, et al: Performance and evaluation of the circular ring transverse axial positron camera (CRTAPC). *IEEE Trans Nucl Sci* NS-24, No 1:532–543, 1977
4. ERIKSSON L, BOHM C, BERGSTROM M, et al: One year experience with a high resolution ring detector positron camera system: present status and future plans. *IEEE Trans Nucl Sci* NS-27, No 1:435–444, 1980
5. DERENZO SE, BUDINGER TF, CAHOON JL, et al: High resolution computed tomography of positron emitters. *IEEE Trans Nucl Sci* NS-24, No 1:544–558, 1977
6. DERENZO SE, BUDINGER TF, CAHOON JL, et al: The Donner 280-crystal high resolution positron tomograph. *IEEE Trans Nucl Sci* NS-26, No 2:2790–2793, 1979
7. THOMPSON CJ, YAMAMOTO YL, MEYER E: Positome II: a high-efficiency positron imaging device for dynamic brain studies. *IEEE Trans Nucl Sci* NS-26, No 1:583–589, 1979
8. RICCI AR, HOFFMAN EJ, PHELPS ME, et al: Emission computed tomography simulator. *IEEE Trans Nucl Sci* NS-27, No 1:479–484, 1980
9. BROWNELL G, BURNHAM C, CORREIA J. et al: Transverse section imaging with the MGH positron camera. *IEEE Trans Nucl Sci* NS-26, No 2:2698–2702, 1979
10. MULLANI NA, HIGGINS CS, HOOD JT, et al: PETT IV: design analysis and performance characteristics. *IEEE Trans Nucl Sci* NS-25, No 1:180–183, 1978
11. TER-POGOSSIAN MM, MULLANI NA, HOOD J, et al: A multislice positron emission computed tomograph (PETT IV) yielding transverse and longitudinal images. *Radiology* 128:477–484, 1978
12. TER-POGOSSIAN MM, MULLANI NA, HOOD JT, et al: Design considerations for a positron emission transverse tomograph (PETT V) for imaging of the brain. *J Comput Assist Tomogr* 2:539–544, 1978
13. CARROLL LR: Design and performance characteristics of a production model positron imaging system. *IEEE Trans Nucl Sci* NS-25, No 1:606–614, 1978
14. CHO ZH, NALCIOGLU O, FARUKHI MR: Analysis of a cylindrical hybrid positron camera with bismuth germanate (BGO) scintillation crystals. *IEEE Trans Nucl Sci* NS-25, No 2:952–963, 1978
15. CARROLL LR, HENDRY GO, CURRIN JD: Design criteria for multislice positron emission-computed tomography detector systems. *IEEE Trans Nucl Sci* NS-27, No 1:485–488, 1980
16. DERENZO SE, ZAKLAD H, BUDINGER TF: Analytical study of a high-resolution positron ring detector system for transaxial reconstruction tomography. *J Nucl Med* 16:1166–1173, 1975
17. BECK RN: A theory of radioisotope scanning systems. In *Medical Radioisotope Scanning*. vol 1, Vienna, IAEA, 1964, pp 35–56
18. BUDINGER TF, DERENZO SE, GREENBERG WL, et al: Quantitative potentials of dynamic emission computed tomography. *J Nucl Med* 19:309–315, 1978
19. DERENZO SE: Tabulation of side shielding optimization and comparison of detector materials for circular positron emission tomographs. Berkeley, CA., Lawrence Berkeley Lab. Report LBL-9584, 1980
20. DERENZO SE: Monte Carlo calculations of the detection efficiency of linear arrays of NaI(Tl), BGO, CsF, Ge(Li) and plastic for 511 keV photons. Berkeley, CA., Lawrence Berkeley Lab. Report LBL-9201, 1980
21. ANGER HO: Survey of radioisotope cameras. *ISA Trans* 5: 311–334, 1966
22. NICKLES RJ, MEYER HO: Design of a three-dimensional positron camera for nuclear medicine. *Phys Med Biol* 23: 686–695, 1978
23. ALLEMAND R, GRESSET C, VACHER J: Potential advantages of a cesium fluoride scintillator for a time-of-flight positron camera. *J Nucl Med* 21:153–155, 1980
24. MULLANI NA, FICKE DC, TER-POGOSSIAN MM: Cesium fluoride: a new detector for positron emission tomography. *IEEE Trans Nucl Sci* NS-27, No 1:572–575, 1980
25. CHU D, TAM KC, PEREZ-MENDEZ V, et al: High-efficiency collimator-converters for neutral particle imaging with MWPC. *IEEE Trans Nucl Sci* NS-23, No 1:634–639, 1976
26. NEUMANN MJ: A gas-filled channel converter for fast coincidence cameras. *IEEE Trans Nucl Sci* NS-24, No 1: 515–520, 1977
27. JEAVONS AP, TOWNSEND DW, FORD NL, et al: A high-resolution proportional chamber positron camera and its applications. *IEEE Trans Nucl Sci* NS-25, No 1:164–173,

1978
28. LUM GK, GREEN MI, PEREZ-MENDEZ V, et al: Lead oxide glass tubing converters for gamma detection in MWPC. *IEEE Trans Nucl Sci* NS-27, No 1:157-165, 1980

SOCIETY OF NUCLEAR MEDICINE
COMPUTER COUNCIL ANNUAL MEETING
INSTRUMENTATION COUNCIL MEETING

February 6-7, 1981 **Marriott Hotel** **New Orleans, Louisiana**

The Computer Council and Instrumentation Council of the Society of Nuclear Medicine will meet February 6 and 7, 1981 at the Marriott Hotel in New Orleans, Louisiana.

A topical symposium is being sponsored by the SNM Computer Council consisting of invited presentations, contributed papers, educational sessions, and active attendee participation. Submitted papers are encouraged on Functional Mapping of Organ Systems. Submitted papers will also be considered in other aspects of the use of instruments and computers in nuclear medicine.

The Councils welcome the submission of abstracts from members and nonmembers of the Society of Nuclear Medicine. The title, author, and institutional affiliations should be included at the top of the first page. The name of the author presenting the paper must be underlined. Abstracts should contain a statement of purpose, the methods used, results, and conclusion.

Original abstracts and supporting data should be sent in duplicate to:

Computer Council
Ronald R. Price, Ph.D.
Dept. of Radiology and Radiological Sciences
Vanderbilt University Medical Center
Nashville, TN 37232
Phone: (615) 322-2394

Instrumentation Council
L. Stephen Graham, Ph.D.
Nuclear Medicine Service
Veterans Administration Medical Center
16111 Plummer
Sepulveda, CA 91343
Phone: (213) 891-2485

Abstracts must be received no later than October 1, 1980.